Electronic Supplementary Material (ESI) for Sustainable Energy & Fuels.

Graphene oxide mediated scalable preparation of heterostructured MoS_2-MoO_3/Graphene nanohybrids for efficient energy storage application

Sunil P. Lonkar[1,] and Saeed M. Alhassan[2,*]*

[1]Advanced Materials Research Center (AMRC), Technology Innovation Institute (TII), P.O.Box: 9639, Abu Dhabi, United Arab Emirates

[2]Department of Chemical Engineering, Khalifa University, P.O box 127788, Abu Dhabi, UAE

E-mail: saeed.alkhazraji@ku.ac.ae; sunil.lonkar@ku.ac.ae

Tel:+971-26075944, Fax: +971-26075200

Materials

Ammonium tetrathiomolybdate [ATTM; $(NH_4)_2MoS_4$], elemental sulfur, activated carbon (AC), and potassium hydroxide (KOH) were purchased from Sigma-Aldrich and were used as received without further purification.

Characterizations

The structural and morphological characterization of the resulting 3D MoS_3/RGO nanohybrids were performed by various sophisticated tools and techniques. The morphology was investigated by scanning electron microscope (SEM, 1540 XB Zeiss equipped with energy dispersive X-ray analysis, EDX) and transmission electron microscopy (TEM, FEI Tecnai G20 with 0.11 nm point resolution and operated at 200 kV using Gatan digital camera). The crystalline structure was elucidated by X-ray diffraction (XRD, Philips X'Pert Pro X-Ray diffractometer equipped with graphite-monochromated Cu Kα radiation at λ = 1.541 Å, 2θ=5-60°). X-ray photoelectron spectroscopy (XPS) spectra were recorded on SSX-100 system (Surface Science Laboratories, Inc. equipped with a monochromated Al K_α X-ray source, a hemispherical sector analyzer, and a resistive anode detector). The Raman spectroscopy was performed on LabRAM HR (Horiba Scientific) using a 633 nm laser excitation line. The surface property features were studied using BET analysis, N_2 physisorption was carried out at liquid N_2 temperature with a Micromeritics ASPS 2010 analyzer to examine the porosity and surface area of the hybrids. The samples were pretreated at 100 ^oC in a high vacuum for 24 h before N_2 adsorption.

Electrochemical Measurements

The specific capacitance of the electrodes under materials was calculated by using the GCD data under three-electrode (Csp, $F \cdot g^{-1}$) was calculated by using the following the Eq. S1, respectively [1]:

$$C_{sp} = \frac{I\Delta t}{m\Delta V} \quad \text{(S1)}$$

Where 'I' is the discharge current in Ampere (A), 'Δt' is the discharge time in seconds (s), m is the active material mass in grams (g), and 'ΔV' is the working potential window in Volts (V).

To achieve optimal electrochemical performance, the mass ratio of positive and negative electrode is received according to eq.S2[2]:

$$\frac{m^+}{m^-} = \frac{C_{sp}^-}{C_{sp}^+} \times \frac{\Delta V^-}{\Delta V^+} \quad \text{(S2)}$$

herein, m (g) is the mass loading, C_{sp} ($F\ g^{-1}$) is the specific capacitance, ΔV (V) is the discharge voltage range for the positive (+) and negative (−) electrodes.

The specific capacitance of asymmetric cell device ($Csp_{(cell)}$, $F \cdot g^{-1}$) was also calculated by using equation (S1), using m as the total mass of positive and negative electrodes, and the applied potential window. Further, the energy density (E, $Wh \cdot kg^{-1}$) and power density (P, $kW \cdot kg^{-1}$) of the resulting asymmetric device was estimated by using equation S4 and S5, respectively 2.

$$C_{sp\ (cell)} = \frac{I\Delta t}{(m^- + m^+)\Delta V} \quad \text{(S3)}$$

$$E = \frac{1}{2} C_{sp(cell)} \times \Delta V^2 \times \frac{1}{3.6} \quad \text{(S4)}$$

$$P = \frac{E}{\Delta t} \times 3.6 \quad \text{(S5)}$$

Where, the capacitance '$C_{sp(cell)}$' ($F \cdot g^{-1}$) is asymmetric cell-specific capacitance obtained from Eq.S3 and m^+ and m^- is the mass of negative and positive electrodes, respectively, ΔV (V) is the operating voltage range, and Δt (s) is the discharge time estimated from the GCD profiles. The

cyclic stability of the electrodes was evaluated by 5000 GCD cycles of the individual electrode and 3000 GCD cycles of asymmetric supercapacitor at 3 A g^{-1} in the range of 0 to 1.8 V.

HER Mechanism:

The recorded potentials were transformed into reversible hydrogen electrode (RHE) based on the following Eq.S6:

$$E_{RHE}\,(V) = E_{SCE}\,(V) + 0.059pH + E^{0}_{SCE}\,(V) \qquad (S6)$$

where the E_{RHE} is the transformed potential vs. RHE, E_{SCE} is the applied potential vs. Hg/Hg_2Cl_2 reference electrode, and E^{0}_{SCE} is the standard potential of SCE electrode at 25 °C (i.e., 0.241 V).

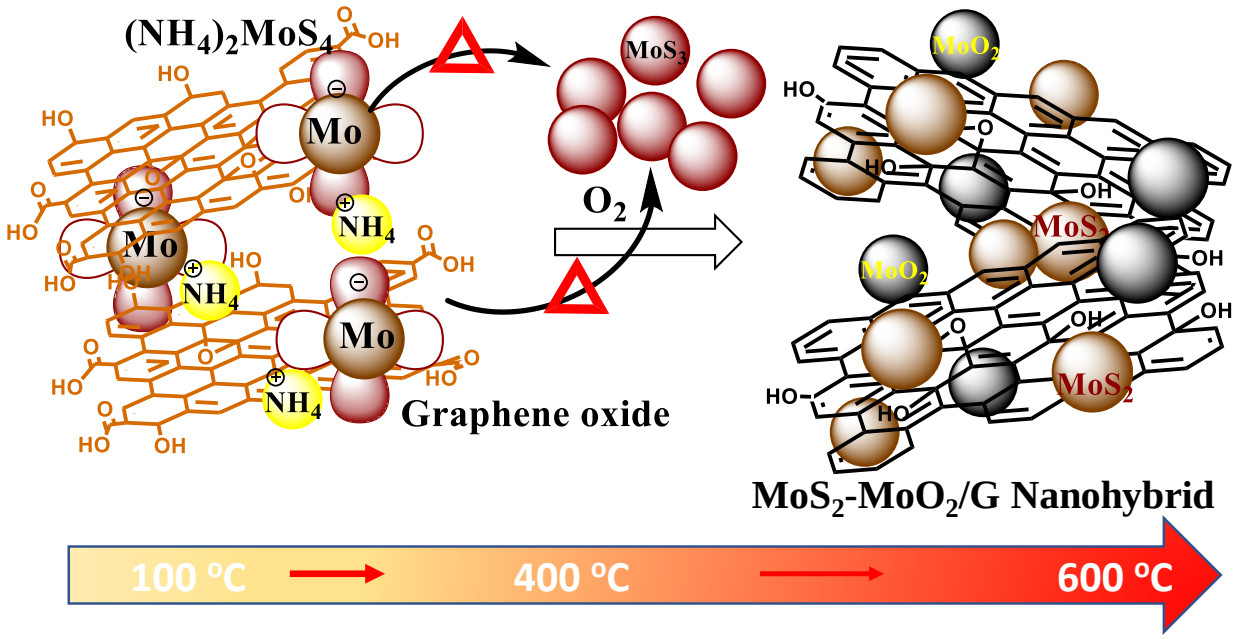

Scheme S1: Schematic illustration of formation of MoS_2-MoO_2/graphene nanohybrid

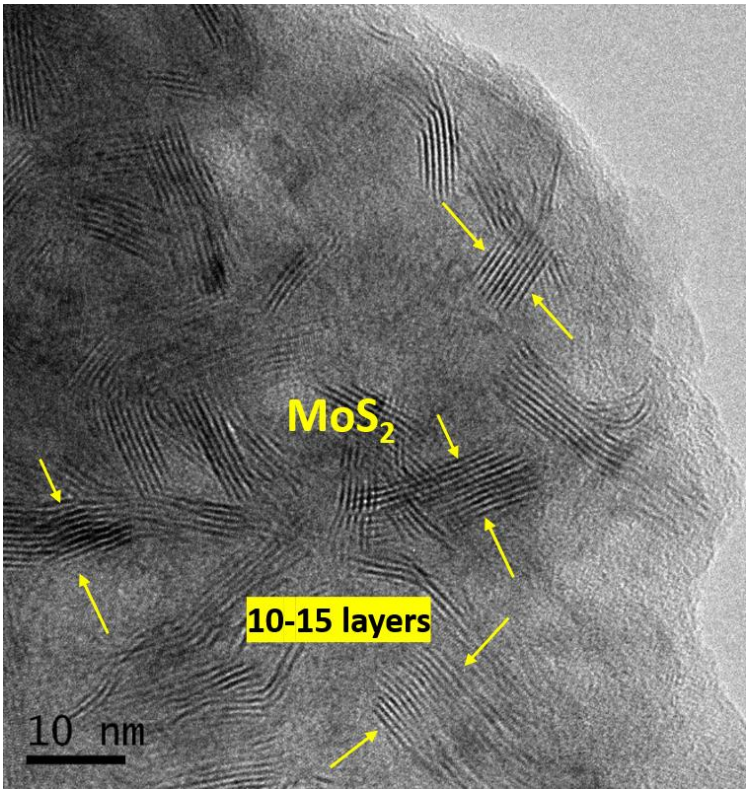

Figure S1. TEM images of pristine MoS_2 nanoparticles

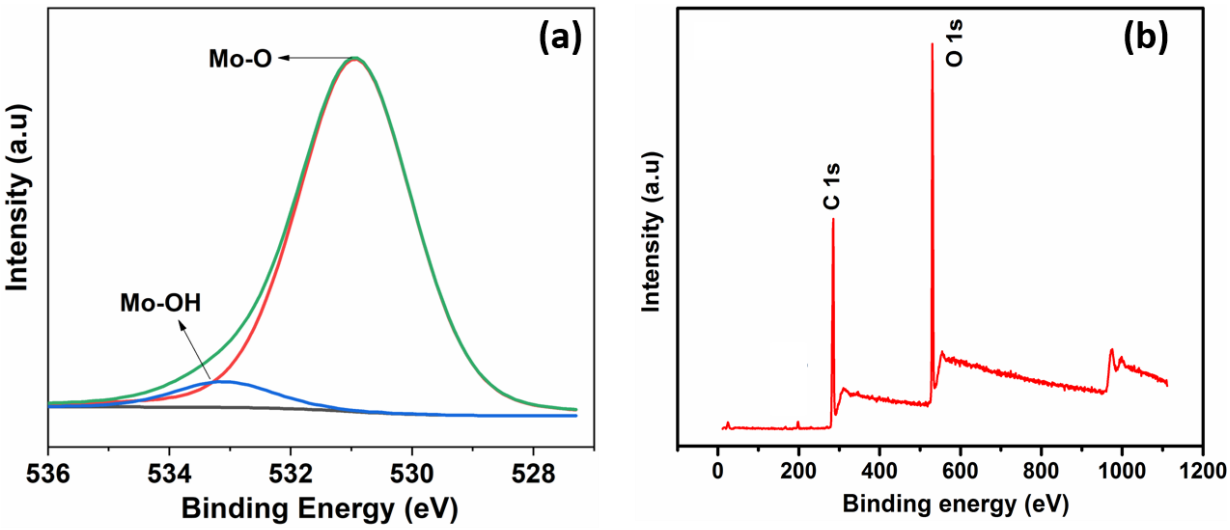

Figure S2. XPS deconvoluted spectra of O 1s (a) and XPS survey spectra of pristine GO (b).

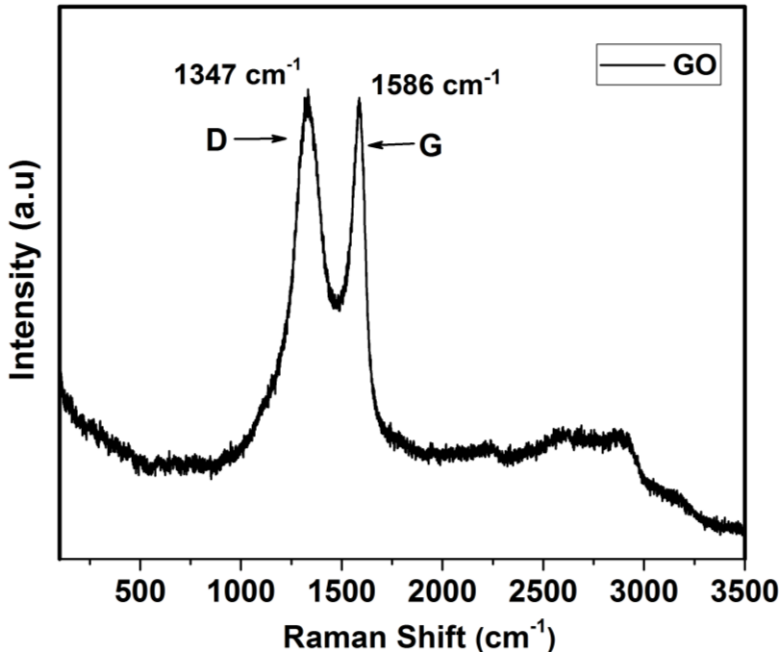

Figure S3. Raman spectra of pristine GO.

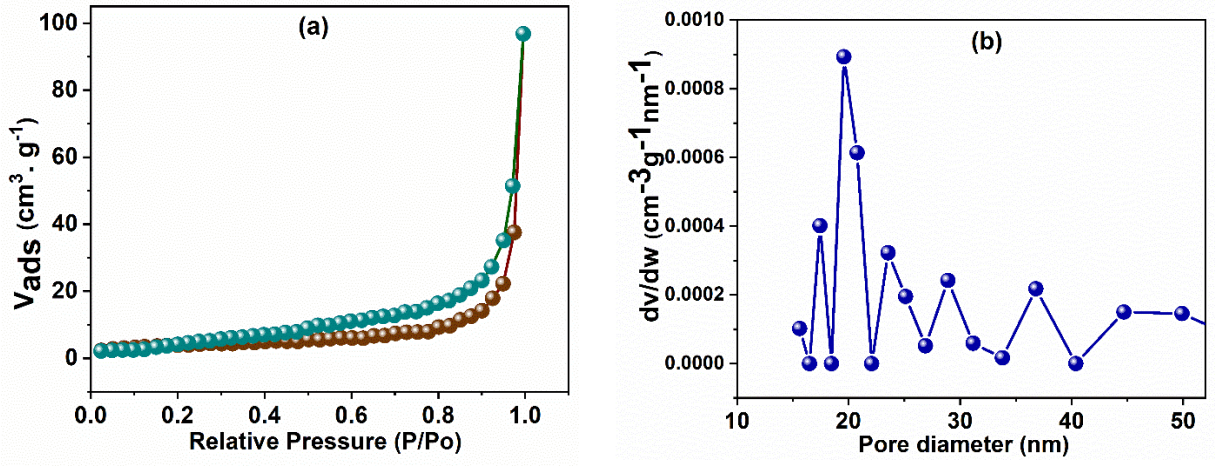

Figure S4. N_2 adsorption-desorption isotherms (a) and BJH pore size distribution curves (b) for pristine MoS_2 nanoparticles.

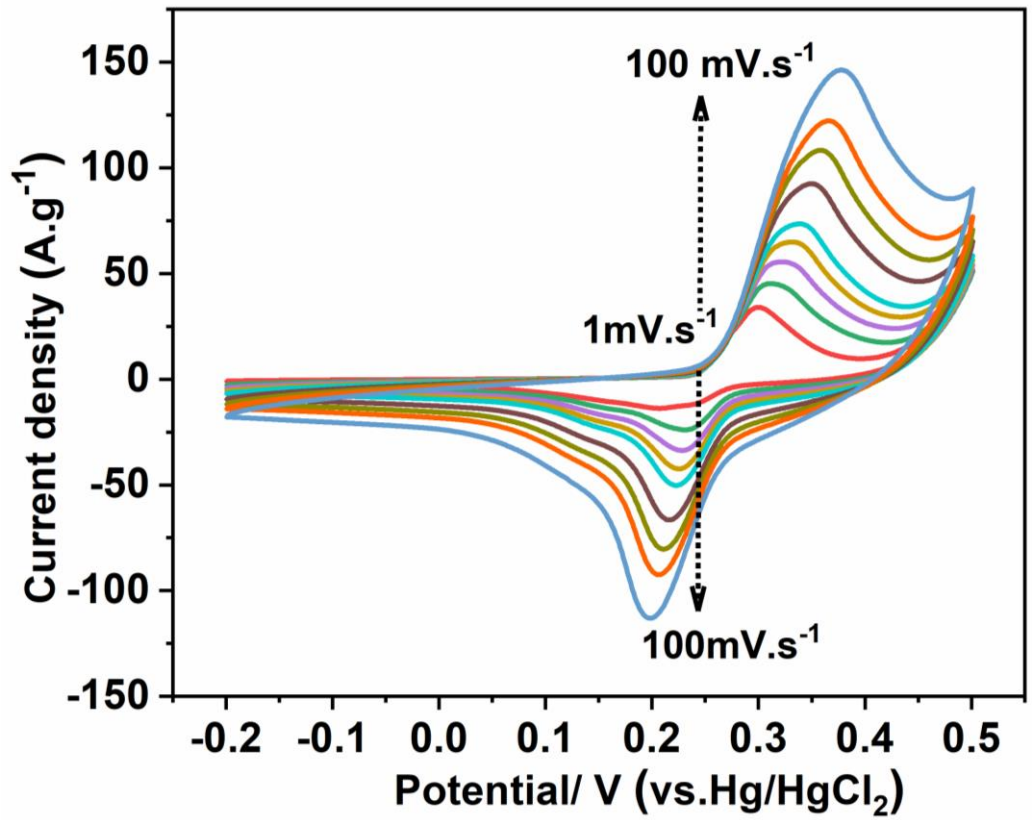

Figure S5. CV curve of pristine MoS_2 nanoparticles at different scan rates.

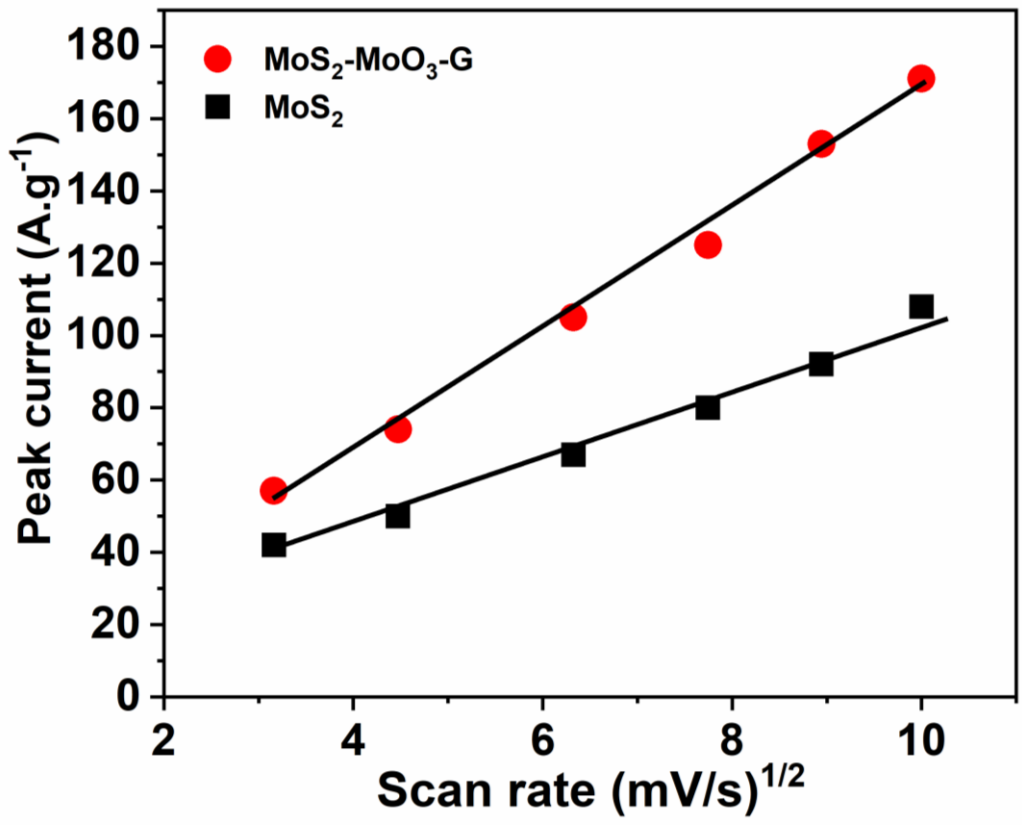

Figure S6. Fittings of anodic peak current vs. the square root of scan rate for MoS_2-MoO_2/G nanohybrid and pristine MoS_2.

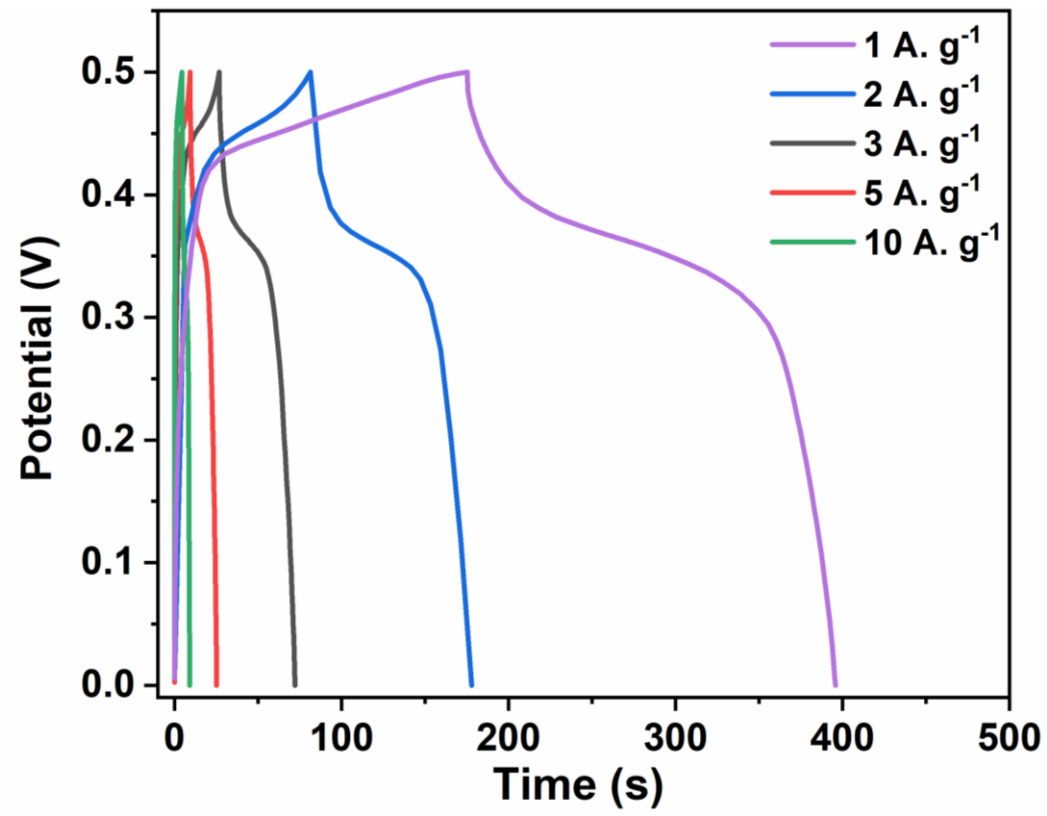

Figure S7. Galvanostatic charge/discharge curves of MoS_2 at different current densities.

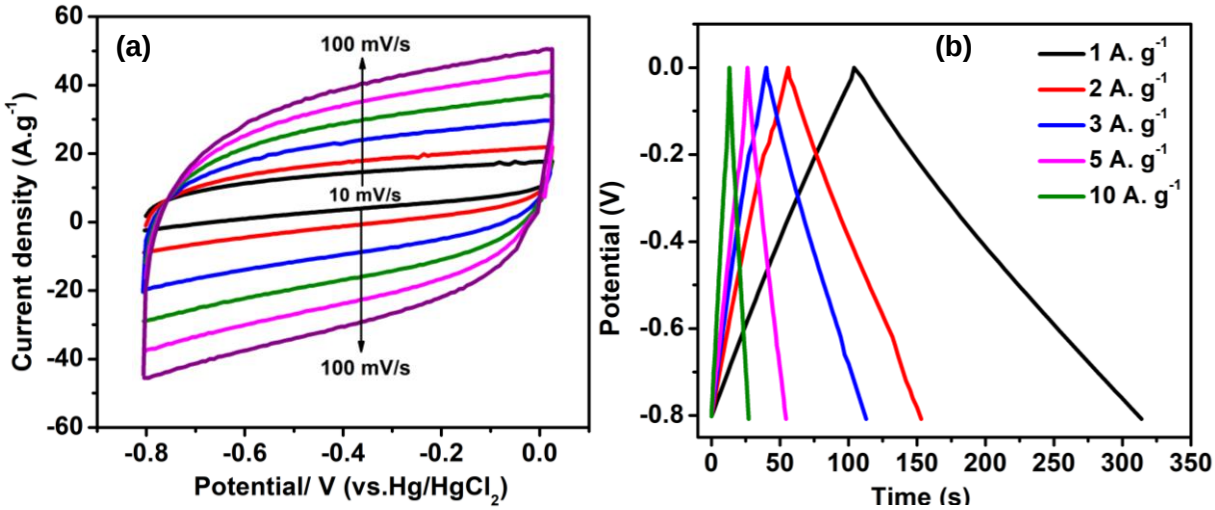

Figure S8. CV curve at different scan rate (a) and GCD curves at different current densities of AC electrode.

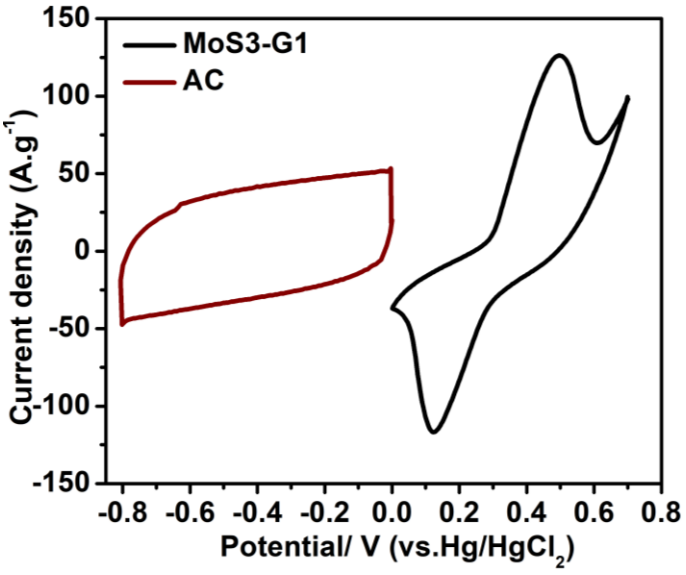

Figure S9. Cyclic voltammetry (CV) curves of the 3D MoS_3-G nanohybrid and active carbon (AC) as working electrodes in three-electrode system.

Table S1. Comparison of specific capacitance and cycle stability of recently reported MoS_2 /MoO_x hybridized and carbon-based electrode materials.

Active material	**Method**	**Specific capacitance (F g^{-1})**	**Capacitance retention (%)/cycles**	**Reference**
MoS_2/MoO_2/CNT	Microwave-Solid state	266.1 (1 A g^{-1})	128/2500	[3]
MoS_2/MoO_3	Hydrothermal	287.7 (1 A g^{-1})	90 /1000	[4]
MoO_2/MoS_2	Hydrothermal	433.3 (5 mV s^{-1})	84.41 / 5000	[5]
MoS_2/MoOx/Carbon	Microwave-assisted hydrothermal	230 (5 mV s^{-1})	128 /1500	[6]
PANI/MoO_3 /ACC	Hydrothermal/In-situ polymerization reactions	1050 (0.5 A g^{-1})	71/ 2000)	[7]
MoS_2/MoO_3/PPy	Microwave-assisted hydrothermal method	527 F (5 mV s^{-1})	-	[8]
MoS_2/RGO	Hydrothermal	607 (5 mV s^{-1})	95/1000)	[9]
Carbon@MoS_2/MoO_2	Hydrothermal/ Calcination	569 (1 A g^{-1})	91.4 (5000)	[10]
MoO_3/Carbon cloth (CC)	Magnetron sputtering	240 (1.5 A g^{-1})	78.5 /5000	[11]
MoS_2/MoO_3@graphite	Microwave	268 (1 A g^{-1})	83/6000	[12]
MoS_2-MoO_3/Graphene	Solid-State, Thermal	872 (1 A g^{-1})	98 /3000	Present work

Table S2. Comparison of the catalytic performances involving MoS_2 and MoOx nanostructured hybrid materials for HER.

Catalysts	**Electrolyte**	**Overpotential (mV) @ 10 mA.cm^2**	**Tafel slope (mV dec^{-1})**	**Reference**
MoS_2@Ni/CC	1M KOH	191	89	[13]
MoS_2/Ni_3S_2 heterostructures	1 M KOH	249	110	[14]
MoS_2/G HS	1 M KOH	183	127	[15]
NiS/MoS_2 CC	1 M KOH	106	56.7	[16]
MoO_{3-x}	0.1M KOH	143	56	[17]
MoS_2@NiO	1 M KOH	226	43	[18]
Few-layered MoS_2 nanosheets	1 M NaOH	350	105	[19]
Porous MoO_3	1M KOH	113	95	[20]
MoS_2-MoO_3/Graphene	Solid-State, Thermal	93	63	Present work

References

1 P. Asen, M. Haghighi, S. Shahrokhian and N. Taghavinia, *J. Alloys Compd.*, , DOI:10.1016/j.jallcom.2018.12.176.

2 Y. Shao, M. F. El-Kady, J. Sun, Y. Li, Q. Zhang, M. Zhu, H. Wang, B. Dunn and R. B. Kaner, *Chem. Rev.*, 2018.

3 Y. Tian, H. Du, M. Zhang, Y. Zheng, Q. Guo, H. Zhang, J. Luo and X. Zhang, *J. Mater. Chem. C*, , DOI:10.1039/c9tc02391g.

4 S. V. P. Vattikuti, P. C. Nagajyothi, P. Anil Kumar Reddy, M. Kotesh Kumar, J. Shim and C. Byon, *Mater. Res. Lett.*, , DOI:10.1080/21663831.2018.1477848.

5 T. Zhang, L. Bin Kong, M. C. Liu, Y. H. Dai, K. Yan, B. Hu, Y. C. Luo and L. Kang, *Mater. Des.*, , DOI:10.1016/j.matdes.2016.09.054.

6 F. N. I. Sari and J. M. Ting, *ChemSusChem*, , DOI:10.1002/cssc.201702295.

7 J. Ling, H. Zou, W. Yang, W. Chen, K. Lei and S. Chen, *J. Energy Storage*, , DOI:10.1016/j.est.2018.09.007.

8 F. N. Indah Sari and J. M. Ting, *Electrochim. Acta*, , DOI:10.1016/j.electacta.2019.07.044.

9 S. Dutta and S. De, in *Materials Today: Proceedings*, 2018.

10 J. Tian, H. Zhang and Z. Li, *ACS Appl. Mater. Interfaces*, , DOI:10.1021/acsami.8b08534.

11 D. Murugesan, S. Prakash, N. Ponpandian, P. Manisankar and C. Viswanathan, *Colloids Surfaces A Physicochem. Eng. Asp.*, , DOI:10.1016/j.colsurfa.2019.02.062.

12 Y. Tian, X. Yang, A. Nautiyal, Y. Zheng, Q. Guo, J. Luo and X. Zhang, *Adv. Compos. Hybrid Mater.*, , DOI:10.1007/s42114-019-0075-4.

13 Z. Xing, X. Yang, A. M. Asiri and X. Sun, *ACS Appl. Mater. Interfaces*, , DOI:10.1021/acsami.6b02331.

14 Y. Yang, K. Zhang, H. Lin, X. Li, H. C. Chan, L. Yang and Q. Gao, *ACS Catal.*, , DOI:10.1021/acscatal.6b03192.

15 X. Yu, G. Zhao, S. Gong, C. Liu, C. Wu, P. Lyu, G. Maurin and N. Zhang, *ACS Appl. Mater. Interfaces*, , DOI:10.1021/acsami.0c04838.

16 S. Guan, X. Fu, Z. Lao, C. Jin and Z. Peng, *Sustain. Energy Fuels*, 2019, **3**, 2056–2066.

17 Z. Luo, R. Miao, T. D. Huan, I. M. Mosa, A. S. Poyraz, W. Zhong, J. E. Cloud, D. A. Kriz, S. Thanneeru, J. He, Y. Zhang, R. Ramprasad and S. L. Suib, *Adv. Energy Mater.*, , DOI:10.1002/aenm.201600528.

18 Z. H. Ibupoto, A. Tahira, P. Tang, X. Liu, J. R. Morante, M. Fahlman, J. Arbiol, M. Vagin and A. Vomiero, *Adv. Funct. Mater.*, 2019, **29**, 1807562.

19 B. Lai, S. C. Singh, J. K. Bindra, C. S. Saraj, A. Shukla, T. P. Yadav, W. Wu, S. A. McGill, N. S. Dalal, A. Srivastava and C. Guo, *Mater. Today Chem.*, 2019, **14**, 100207.

20 M. Zhang, R. Li, D. Hu, X. Huang, Y. Liu and K. Yan, *J. Electroanal. Chem.*, 2019, **836**, 102–106.